

# Insulating potential shape created by ultrathin silicon oxide layers

© E.I. Goldman, G.V. Chucheva<sup>†</sup>, I.A. Shusharin

Fryazino Branch of the Kotelnikov Institute of Radioengineering and Electronics, Russian Academy of Sciences,  
141190 Fryazino, Russia

<sup>†</sup>E-mail: gvc@ms.ire.mssi.ru

Received October 18, 2021

Revised November 20, 2021

Accepted November 20, 2021

A previously developed method for reconstructing the insulating potential pattern created by an ultrathin silicon oxide layer from the field dependences of the tunneling current has been modernized. Trapezoidal model potential parameters, that provide the dependence of the current-to-voltage logarithm derivative as close as possible to the experimental one, have been calculated. The approach to starting successive iterations of the potential has been changed in such a way that the functions calculated using the model shape are used rather than zeroing the first turning point coordinates in zero-order approximation. The modernized algorithm has been applied to the experimental field current dependences in  $n^+$ -Si-SiO<sub>2</sub>- $n$ -Si structures with an oxide thickness of 3.7 nm, that have a pronounced asymmetry of the tunneling current-voltage characteristics with respect to the external voltage polarity. The effective potential barrier reconstructed from the experimental data is always significantly thinner than the insulating layer, with its maximum shifted towards the contact with the polycrystalline material, and the effective mass of the tunneling electron is several times greater than the typical for thick silicon oxide.

**Keywords:** degenerate polysilicon-silicon oxide-silicon, ultrathin oxide, tunneling current-voltage characteristics, potential pattern.

DOI: 10.21883/SC.2022.03.53065.9756

## 1. Introduction

Ultrathin (< 5 nm thick) silicon oxide layers are currently and for the foreseeable future the main insulating material used for creation of existing and new nanoelectronic structures [1]. As opposed to thick oxides, the shape of the insulating potential created by ultrathin SiO<sub>2</sub> cannot be treated as rectangular. The problem is that silicon oxide is a disordered material and its atomic structure does not interface the crystal lattices of semiconductors used to make active nanoelectronic components. Therefore, a transition layer occurs at the semiconductor-silicon oxide interface (IF), whereby the minimum thickness of the transition layer for Si-SiO<sub>2</sub> contact is equal to 2 atomic layers [2]. Since the transitions between the crystal Si and SiO<sub>2</sub> and between the oxide and other semiconductor, e.g. a poly-Si one, in total occupy less than 35% of the ultrathin dielectric volume [2], they actually define the insulator properties to a great extent. The thinner the insulator is, the higher the transition layer content in the insulator is. Substrate-to-oxide and oxide-to-polysilicon contacts are created in different processes and have different crystal structure. Therefore, coordinate dependences of the insulating potential pattern with a different shape (asymmetric) can be also expected at these interfaces. Depending on the manufacturing process, oxide has different insulating properties. Minimum conductivity associated with tunneling through the dielectric layer is achieved at SiO<sub>2</sub> obtained by means of dry high-temperature silicon oxidation [3]. The purpose of the investigation was to create an actual insulating potential pattern from current-voltage

characteristics (CVC) of ultrathin SiO<sub>2</sub> layers with tunneling type conductivity.

An important consideration shall be noted: there are no theoretical grounds that allow to assume the electron wave function for a disordered material as a product of gradually-varied amplitude and oscillating function at atomic spacing that is typical of the effective mass method [4]. However, this is the assumption that is used by the absolute majority of researchers in the field of electron effects at the semiconductor-SiO<sub>2</sub> interface. In the framework of such assumptions, model calculations of various quantum effects [5] were carried out as early as the last century, and by now a branched computer-aided calculation area has been formed to ensure design and creation of nanometer range electronic devices [6]. The effective mass equation used to describe the effects at the oxide interface means that the potential coordinate dependences in the isolating distance and tunneling electron mass  $m$  included in the equation shall be a kind of values leading to the achievement of results that coincide the experimental results. Because of the absence of data on the effective potential pattern, calculations are generally performed using a rectangular potential shape (trapezoidal in the external field) and  $m = 0.5m_0$  typical of thin oxide,  $m_0$  is a free electron mass. That's why such investigations result in inaccurate determination of the electron wave function penetration into the insulating layer [7] and, thus, to partial matching of theoretical and experimental data. Therefore, an important physical problem involves plotting of dependences of the insulating potential vs. the tunneling electron coordinate and mass using experimental

tunneling current-voltage characteristics (CVC) of ultrathin SiO<sub>2</sub> layers. Such experimental data handling problem was solved earlier in [7]. In this publication, an apparatus developed before will be slightly modified and applied to the silicon–ultrathin oxide–poly-*n*<sup>+</sup>-silicon structure samples similar to those investigated in [7], but with a pronounced asymmetry of tunnel CVC [8].

## 2. Apparatus for potential pattern reconstruction from field dependences of tunneling current through an ultrathin insulating layer

Tunneling CVC of the *n*-Si–ultrathin SiO<sub>2</sub>–*n*<sup>+</sup>-Si structures will be addressed. In conditions when the insulating barrier (see Fig. 1) is low transparent to probable tunneling via oxide *D*, the following quasiclassical expression is true

$$D(V, E_{\perp}) = \exp(-\Phi),$$

$$\Phi(V, E_{\perp}) = \left(\frac{8m}{\hbar^2}\right)^{(1/2)} \int_{z_1}^{z_2} \left[U(z) - E_{\perp} - qV \frac{z}{h}\right]^{(1/2)} dz. \quad (1)$$

Here,  $\hbar$  is the Planck's constant;  $U(z)$  is the desired potential pattern in the oxide layer  $0 < z < h$  measured from the Fermi level of the electron-injecting degenerate *n*<sup>+</sup>-Si ( $z < 0$ );  $z$  is a coordinate on the normal to the Si-SiO<sub>2</sub> interface plane,  $z > h$  is the *n*-Si region;  $q$  is an elementary charge;  $V$  is an external electric field voltage drop on an insulator with thickness  $h$ ;  $E_{\perp}$  is a tunneling electron energy corresponding to the perpendicular movement;  $z_1(V)$  and  $z_2(V)$  are turning point coordinates. For subdivision of the potential in the insulator into two components — self field with pattern  $U(z)$  and external field  $qV(z/h)$  — voltage  $V$  reference point shall be defined. Assume that in equilibrium  $V = 0$ . Then, potential  $U(z)$  shall contain contributions both from charges fixed in the insulating distance and from the field electrode–semiconductor contact potential difference. In ultrathin insulating layers between confined states concentrated inside SiO<sub>2</sub> and conductivity regions *n*-Si and *n*<sup>+</sup>-S, intense electron exchange takes place.

As a result, when voltage  $V$  is increased, charge state of only electron traps concentrated in close vicinity to the Si-SiO<sub>2</sub> interface is changed significantly. Therefore, the external field distribution over the insulator will be assumed as  $qV(z/h)$  [see the second equation (1)].

As shown in [7,9], 3.7 nm barrier transparency grows by a factor of  $e = 2.71 \dots$  with an increase in the tunneling level, when the energy  $E_{\perp}$  is increased by  $E_0 \sim 0.055$  eV. This value is much greater than the energy distances between the adjacent electron quantum levels in the enrichment layer [5], but is considerably lower than the scope of potential variation ( $\sim 3$  eV). The enrichment bend of regions in *n*-Si at the oxide interface also changes insignificant with

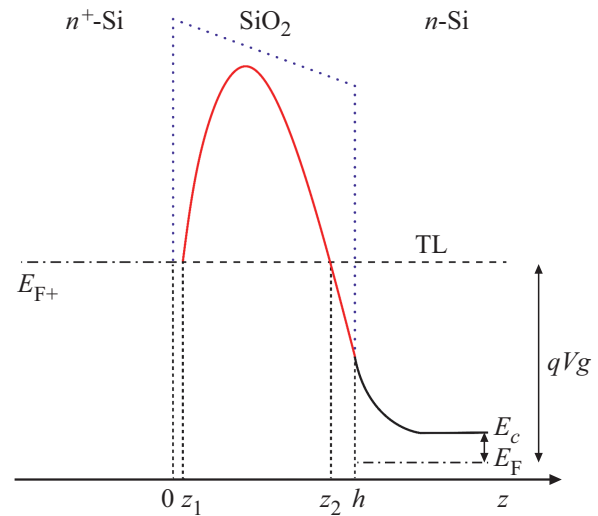


**Figure 1.** Potential pattern of the *n*<sup>+</sup>-Si–SiO<sub>2</sub>–*n*-Si structure in the external field. Solid line is the actual potential pattern, dotted line is the trapezoidal (rectangular) barrier model, dot-and-dash line is the Fermi level, TL is the electron tunneling level,  $E_c$  is the bottom of conduction band of *n*-silicon,  $E_F$  is the Fermi energy in *n*-Si,  $E_{F+}$  is the Fermi level in *n*<sup>+</sup>-Si.

the external field as compared to the tunnel barrier height. Therefore, in order to achieve an actual potential pattern in the oxide layer as also described in [7], the following expression will be used to describe the dependence of current  $J$  vs. voltage  $V$

$$J = \bar{J} \cdot D(V, 0). \quad (2)$$

Here,  $\bar{J}$  is a preexponential factor whose dependence on voltage will be also neglected. Thus, due to a small amplitude, tunneling current oscillations caused by the electron wave interference in the range between the turning point in oxide and SiO<sub>2</sub>-Si interface will be also omitted [10,11]. Function  $U(z)$  will be represented parametrically — through two branches of dependences of turning point coordinated vs. voltage:  $z = z_1(V)$ ,  $U = qV[z_1(V)/h]$  at  $z_1(V) < z_m$  and  $z = z_2(V)$ ,  $U = qV[z_2(V)/h]$  at  $z_2(V) > z_m$ ;  $z = z_m$  is a point coordinate where the barrier disappears with the external field growth at  $V = V_m$ . Now expression (1) for  $\Phi(V, 0)$  is transformed as

$$\Phi = \frac{1}{\bar{V}^{(1/2)}} \int_V^{V_m} (V' - V)^{(1/2)} \left(-\frac{df}{dV'}\right) dV',$$

$$f(V) = \left\{ \left[\frac{z_2(V)}{h}\right]^{3/2} - \left[\frac{z_1(V)}{h}\right]^{3/2} \right\}. \quad (3)$$

Here,  $\bar{V} = (9\hbar^2/32mh^2q)$ ,  $V_m$  is the barrier removal voltage.

Equation (3) was transformed in [7]:

$$\begin{aligned} f(V) &= \frac{2\bar{V}^{(1/2)}}{\pi} \int_V^{V_m} (V' - V)^{-(1/2)} \left[ -\frac{d\Phi(V')}{dV'} \right] dV' \\ &= \frac{4\bar{V}^{(1/2)}}{\pi} \int_0^{x_m} [-\bar{\Phi}(V + x^2)] dx, \end{aligned} \quad (4)$$

where  $\bar{\Phi}(V) = d\Phi/dV$ ,  $x = (V' - V)^{(1/2)}$ ,  $x_m = (V_m - V)^{(1/2)}$ . A summary of  $U(z)$  dependence plotting algorithm from the experimental function  $f(V)$  offered in [7] is given below. 2 CVC branches are measured: semiconductor depletion (injection from poly-Si) — depl index and silicon enrichment (injection from Si) — enr index. 2 functions  $f_{\text{depl}}(V)$  and  $f_{\text{enr}}(V)$  are expressed, respectively, from the experimental curves  $\bar{\Phi}_{\text{depl}}(V)$  and  $\bar{\Phi}_{\text{enr}}(V)$  using equation (4). For each tunneling electron mass from some set covering the range of possible values  $m$ , four sequences are introduced with number  $n$  of dependences  $U_{\text{depl}}^{(n)}(\frac{z}{h})$ ,  $\frac{z_{\text{depl}}^{(n)}(V)}{h}$  and  $U_{\text{enr}}^{(n)}(\frac{z}{h})$ ,  $\frac{z_{\text{enr}}^{(n)}(V)}{h}$ . The specified functions with  $(n + 1)$ -th number are calculated parametrically from  $n$ -th numbers using the following equations:

$$\begin{aligned} U_{\text{depl}}^{(n+1)} &= qV \left\{ f_{\text{depl}}(V) + \left[ \frac{z_{\text{1depl}}^{(n)}(V)}{h} \right]^{3/2} \right\}^{2/3}, \\ \frac{z}{h} = \frac{z_{\text{depl}}^{(n+1)}}{h} &= \left\{ f_{\text{depl}}(V) + \left[ \frac{z_{\text{1depl}}^{(n)}(V)}{h} \right]^{3/2} \right\}^{2/3}, \end{aligned} \quad (5)$$

$$\begin{aligned} U_{\text{enr}}^{(n+1)} &= qV \left\{ f_{\text{enr}}(V) + \left[ \frac{z_{\text{1enr}}^{(n)}(V)}{h} \right]^{3/2} \right\}^{2/3} + E_F, \\ \frac{z}{h} = \frac{z_{\text{enr}}^{(n+1)}}{h} &= 1 - \left\{ f_{\text{enr}}(V) + \left[ \frac{z_{\text{1enr}}^{(n)}(V)}{h} \right]^{3/2} \right\}^{2/3}. \end{aligned} \quad (6)$$

Here,  $z_{\text{1depl}}^{(n)}(V)$ ,  $z_{\text{1enr}}^{(n)}(V)$  are the distances from the injecting surface to the first turning point in the potentials,  $U_{\text{enr}}^{(n)}(\frac{z}{h})$  and  $U_{\text{depl}}^{(n)}(\frac{z}{h})$  respectively. Equations (6) include the fact that, for injection from a semiconductor, expressions (1) and (4) shall be used with changed tunneling level and coordinate reference level. Each  $n$  number designates successive approximation of functions  $U_{\text{enr}}^{(n)}(\frac{z}{h})$  and  $U_{\text{depl}}^{(n)}(\frac{z}{h})$  to the desired dependence  $U(\frac{z}{h})$ . Approximation count is stopped as soon as the curves  $U_{\text{enr}}^{(n)}(\frac{z}{h})$  and  $U_{\text{depl}}^{(n)}(\frac{z}{h})$  stop changing with the increase in  $n$  number. Then that pair of branches that merges into a single line as much as possible is selected from the curve for different values  $m$ .  $U_{\text{enr}}^{(n)}(\frac{z}{h})$  and  $U_{\text{depl}}^{(n)}(\frac{z}{h})$ ,

This mass and single curve  $U(\frac{z}{h})$  are the desired ones.

Dependences  $U_{\text{enr}}^{(n)}(\frac{z}{h})$  and  $U_{\text{depl}}^{(n)}(\frac{z}{h})$  calculated from the experimentally found functions  $f_{\text{depl}}(V)$  and  $f_{\text{enr}}(V)$  were discrete in the form of columns values with line numbers  $i$  and  $j$ :  $U_{\text{enr}i}^{(n)}$ ,  $\frac{z_{\text{enr}i}^{(n)}}{h}$ ,  $U_{\text{depl}j}^{(n)}$ ,  $\frac{z_{\text{depl}j}^{(n)}}{h}$ . A linear interpolation method rather than accurate solution of  $U_{\text{depl}}^{(n)}(z) = qV(\frac{z}{h})$  type equations was used for approximate, but faster determination of functions  $z_{\text{1depl}}^{(n)}(V)$ ,  $z_{\text{1enr}}^{(n)}(V)$ . Discrete dependences were initially made  $\tilde{z}_{\text{1depl}}^{(n)}(\tilde{V})$ ,  $\tilde{z}_{\text{1enr}}^{(n)}(\tilde{V})$  according to the following rules:

$$\begin{aligned} \frac{\tilde{z}_{\text{1enr}j}^{(n)}}{h} &= 1 - \frac{z_{\text{depl}j}^{(n)}}{h}, \quad \tilde{V}_j = \frac{h[U_{\text{depl}j}^{(n)} - E_F]}{q[h - z_{\text{depl}j}^{(n)}]}, \\ \frac{\tilde{z}_{\text{1depl}i}^{(n)}}{h} &= \frac{z_{\text{enr}i}^{(n)}}{h}, \quad \tilde{V}_i = \frac{hU_{\text{enr}i}^{(n)}}{qz_{\text{enr}i}^{(n)}}. \end{aligned} \quad (7)$$

When  $V = \tilde{V}_i$ , then  $\tilde{z}_{\text{1depl}i}^{(n)}$  is the exact value of function  $z_{\text{1depl}}^{(n)}(V)$ ; similarly for enrichment branch when  $V = \tilde{V}_j$ , then  $\tilde{z}_{\text{1enr}j}^{(n)}$  is the exact values of function  $z_{\text{1enr}}^{(n)}(V)$ . Then the desired functions were calculated based on the values linearly interpolated from relationships (7):

$$\begin{aligned} \frac{z_{\text{1enr}}^{(n)}(V)}{h} &= \frac{1}{(\tilde{V}_{j+1} - \tilde{V}_j)} \\ &\times \left[ \frac{\tilde{z}_{\text{1enr}j}^{(n)}}{h} (\tilde{V}_{j+1} - \tilde{V}_j) + \frac{\tilde{z}_{\text{1enr}(j+1)}^{(n)}}{h} (\tilde{V} - \tilde{V}_j) \right], \\ \frac{z_{\text{1depl}}^{(n)}(V)}{h} &= \frac{1}{(\tilde{V}_{i+1} - \tilde{V}_i)} \\ &\times \left[ \frac{\tilde{z}_{\text{1depl}i}^{(n)}}{h} (\tilde{V}_{i+1} - \tilde{V}) + \frac{\tilde{z}_{\text{1depl}(i+1)}^{(n)}}{h} (\tilde{V} - \tilde{V}_i) \right]. \end{aligned} \quad (8)$$

Numbers  $i$  and  $j$  of values  $\tilde{z}_{\text{1enr}j}^{(n)}$ ,  $\tilde{V}_j$  and  $\tilde{z}_{\text{1depl}i}^{(n)}$ ,  $\tilde{V}_i$  used in expressions (8) were chosen so that the pairs  $\tilde{V}_i$ ,  $\tilde{V}_{i+1}$  and  $\tilde{V}_j$ ,  $\tilde{V}_{j+1}$  were the nearest ones to the target voltage  $V$ . It shall be noted that due to convergence of branches  $U_{\text{enr}}^{(n)}(\frac{z}{h})$  and  $U_{\text{depl}}^{(n)}(\frac{z}{h})$  with growth of number  $n$ , at some value of  $m$  to the single curve — effective potential pattern  $U(\frac{z}{h})$  — voltages  $\tilde{V}_i$  and  $\tilde{V}_j$  used in equations (8) are getting closer to  $V$ . Therefore, the linear interpolation accuracy (8) will be sufficient to obtain dependence  $U(\frac{z}{h})$ .

### 3. Preparation of data for the use of apparatus for potential pattern reconstruction in ultrathin insulating layer

In actual experiment, measurements are carried out under limitation of high voltages  $V < V_{\text{II}}$  such that no samples

breakdown occur at  $V = V_{II}$ . Generally, the upper limit of the recorded voltages  $V_{II}$  is considerably lower than  $V_m$ . Therefore, the absence of CVC data at  $V > V_{II}$  formally does not allow to find the dependence  $f(V)$  in this range and limits the accuracy of the dependence in the range  $V < V_{II}$ . Subdivide function  $f(V)$  into two parts and rewrite equation (4) as follows

$$f(V) = \bar{f}(V) + \hat{f}(V),$$

$$\begin{aligned} \bar{f}(V) &= \frac{4\bar{V}^{(1/2)}}{\pi} \int_0^{x_{II}} [-\bar{\Phi}(V + x^2)] dx, \\ \hat{f}(V) &= \frac{4\bar{V}^{(1/2)}}{\pi} \int_{x_{II}}^{x_m} [-\bar{\Phi}(V + x^2)] dx, \end{aligned} \quad (9)$$

$x_{II} = (V_{II} - V)^{(1/2)}$ . Part  $\bar{f}(V)$  is accurately defined by the experiment, and dependence  $\hat{f}(V)$  shall be found from the model considerations associated with the experiment. In [7], a model shape of the potential pattern in a form of inclined line  $U_{mod}(z) = (qV_0/h)[\nu z_2(V_0) + (1 - \nu)z]$  was used to plot curve  $\hat{f}(V)$ , where voltage  $V_0$  corresponded to the inflection point of the experimental characteristic  $d^2\bar{\Phi}/dV^2|_{V=V_0} = 0$ , and parameter  $\nu$  was expressed from the experimental data:  $\nu = [(V_{II} - V_0)/V_0] \times \{[\bar{\Phi}(V_0)/\bar{\Phi}(V_{II})]^{(1/2)} - 1\}^{-1}$ . Such approach is not suitable for handling experimental data [8], where the current in semiconductor enrichment conditions is by orders greater than in depletion conditions for samples at the same voltages. For new conditions, introduction of a more general trapezoidal model potential pattern was required:

$$U_{mod}(z) = U_* \times \begin{cases} 0, & 0 < z < a_l - b_l \\ \frac{z - a_l}{b_l} + 1, & a_l - b_l < z < a_l \\ 1, & a_l < z < h - a_r \\ -\frac{z - (h - a_r)}{b_r} + 1, & h - a_r < z < h - (a_r - b_r) \\ 0, & h - (a_r - b_r) < z < h \end{cases}. \quad (10)$$

It shall be noted that the type of dependence  $U_{mod}(z)$  specified by equations (10) includes both transition layers and possible offsets inside the insulator layer. Parameters of this potential  $U_*$ ,  $\frac{a_l}{h}$ ,  $\frac{b_l}{h}$ ,  $\frac{a_r}{h}$ ,  $\frac{b_r}{h}$  shall comply with equations:  $b_l < a_l < h - a_r$ ,  $a_r > b_r$ ; their specific values for each tunneling electron mass were defined from maximum approach of the model  $\bar{\Phi}_{mod}(V)$  and experimental  $\bar{\Phi}(V)$  characteristics. For this purpose, the following functional

was minimized

$$\begin{aligned} \Omega &= \frac{\int_0^{V_{Idepl}} [\dot{\bar{\Phi}}_{depl}(V) - \dot{\bar{\Phi}}_{mod\ depl}(V)]^2 dV}{V_{Idepl}} \\ &+ \frac{\int_0^{V_{Ienr}} [\dot{\bar{\Phi}}_{enr}(V) - \dot{\bar{\Phi}}_{mod\ enr}(V)]^2 dV}{V_{Ienr}}. \end{aligned} \quad (11)$$

Equations calculated from relationship (1) with substitution of  $U(z)$  for  $U_{mod}(z)$  for  $\bar{\Phi}_{mod}(V)$ ,  $\hat{f}(V) = \frac{4\bar{V}^{(1/2)}}{\pi} \times \int_{x_{II}}^{x_m} [-\bar{\Phi}_{mod}(V + x^2)] dx$  are expressed through elementary functions, but are lengthy and, therefore, they are not included herein.

One more modification made herein as compared with [7] was associated with the initiation of successive approximation procedure (5), (6). For this, dependences  $z_{1depl}^{(0)}(V)$ ,  $z_{1enr}^{(0)}(V)$  corresponding to the zero-order approximation shall be specified. In case of almost symmetric barrier  $z_1(V) \ll z_2(V)$ , therefore,  $z_{1depl}^{(0)}(V) = 0$ ,  $z_{1enr}^{(0)}(V) = 0$  were assumed in [7]. Such equations did not allow to ensure convergence of successive approximations herein. Therefore, from model potential (10), following relationships were calculated

$$\begin{aligned} z_{1depl}^{(0)} &= \frac{(a_l - b_l)}{h \left(1 - \frac{qVb_l}{U_*h}\right)}, \\ z_{1enr}^{(0)} &= \frac{(a_r - b_r)}{h \left(1 - \frac{qVb_r}{U_*h}\right)} + \frac{E_F b_r}{U_* h \left(1 - \frac{qVb_r}{U_*h}\right)}, \end{aligned} \quad (12)$$

that were further used, when calculations using equations (5), (6) were initiated. It shall be noted that for model potential (10), the barrier removal voltage were as follows:  $V_m = \frac{U_* h}{qa_1}$  under semiconductor depletion and  $V_m = \frac{(U_* - E_F)h}{qa_r}$  under semiconductor enrichment.

#### 4. Potential pattern reconstruction in ultrathin insulating layer from the experimental current-voltage characteristics

As mentioned above, we will make an effective potential pattern in ultrathin silicon oxide based on the measurements of tunneling CVC [8]. The investigation included Si-MOS-structures with field electrode Al- $n^+$ -Si:P (field electrode area was  $S = 1.6 \cdot 10^{-3} \text{ cm}^{-2}$ ) insulated from (100)  $n$ -Si substrate with an oxide layer with an optical thickness of  $\sim 3.7 \text{ nm}$ , Fermi energy of the electrons in silicon was equal to 0.26 eV. CVC and high frequency capacitance-voltage characteristics (CapVC) of objects were measured at 1 and 0.5 MHz using LCR Agilent E4980A [12]

precision meter. „Simultaneous“ current and capacity fixation at two high frequencies allowed to define external voltage drop in the insulating layer  $V$  in transient conditions and, thus, to obtain the dependences  $\Phi_{\text{depl}}(V)$  and  $\Phi_{\text{enr}}(V)$  required for the investigation (see Fig. 2). The experimental approach established in [8] ensured precise measurement of the external voltage using a sample as compared with quasi-stationary experiments used as a basis in [7].

Processing of the obtained data was started from the establishment of a test set of 10 tunneling electron masses:  $m/m_0 = 0.2, 0.4, \dots, 1.8, 2.0$ , where  $m_0$  is a free electron mass. Functional (11) was minimized separately for each mass by means of enumeration of  $\Omega$  corresponding to different combinations of function parameter values  $U_{\text{mod}}(z)$ . To reduce the computation time, a successive transition scheme was used to ensure transition to even more reduced intervals between the adjacent initial dependence values (10). Coarse grids were initially specified — 6 values for each of the first three parameters and 4 values for each of the remaining two parameters:

$$\begin{aligned} U_* &= 1.5, 2.0, 3.0, 3.5, 4.0 \text{ eV}, \\ \frac{a_l}{h} &= \frac{0.4}{3}, \frac{0.8}{3}, 0.4, \frac{1.6}{3}, \frac{2}{3}, 0.8; \\ \frac{a_r}{h} &= \left( \frac{0.4}{3}, \frac{0.8}{3}, 0.4, \frac{1.6}{3}, \frac{2}{3}, 0.8 \right) \left( 1 - \frac{a_l}{h} \right); \\ \frac{b_l}{h} &= (0.2, 0.4, 0.6, 0.8) \frac{a_l}{h}; \\ \frac{b_r}{h} &= (0.2, 0.4, 0.6, 0.8) \frac{a_r}{h}. \end{aligned}$$

From the calculated functionals  $\Omega$ , minimum  $\Omega_{\text{min}}$  was found and five values of the initial parameters were selected to ensure this minimum number  $\Omega = \Omega_{\text{min}}$ . A finer grid was prepared for specification of initial parameter values. When the value obtained earlier was placed in the center of the coarse grid, than a double grid space was taken around it,

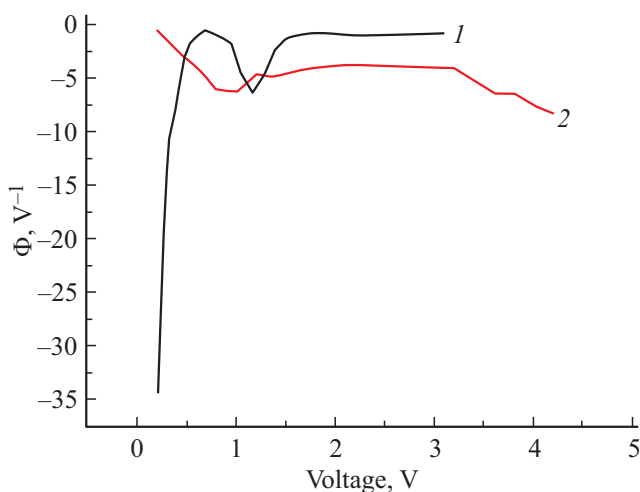


**Figure 2.** Experimental branches of the tunneling current natural logarithm derivatives. 1 —  $\Phi_{\text{depl}}(V)$ , 2 —  $\Phi_{\text{enr}}(V)$ .

Model potential parameter values for  $m = 1.2m_0$

$U_*$	$\frac{a_l}{h}$	$\frac{a_r}{h}$	$\frac{b_l}{h}$	$\frac{b_r}{h}$
3.52 eV	0.18	0.677	0.14	0.024

divided into 7 equal parts, and 6 new values surrounding the values obtained before were selected. When the parameter value found on the coarse grid was located on its edge<sup>1</sup>, then, for a finer grid, a double coarse space was taken with overrunning the old boundary, divided into 7 equal parts and 6 new values were selected. Transition to even finer grids was repeated until value  $(\Omega_{\text{min}}/\Xi)^{1/2}$  began to decrease by lower than 0.05. Here,

$$\Xi = \frac{\int_0^{V_{\text{Idepl}}} [\dot{\Phi}_{\text{depl}}(V)]^2 dV}{V_{\text{Idepl}}} + \frac{\int_0^{V_{\text{Ienr}}} [\dot{\Phi}_{\text{enr}}(V)]^2 dV}{V_{\text{Ienr}}}.$$

data obtained from minimization of functional (11) with  $m = 1.2m_0$  are shown in the table.

This tunneling electron mass value corresponds to the best transition of branches  $U_{\text{enr}}^{(n)}(z)$  and  $U_{\text{depl}}^{(n)}(z)$  into a single effective potential pattern curve (for this see the further paragraphs).

Using the found values of the initial model potential parameters for each  $m$  value from the test set, based on equations (9), a system of functions  $\hat{f}(V)$ ,  $\tilde{f}(V)$  and  $f(V)$  made. Their curves corresponding to  $m = 1.2m_0$  are shown in Fig. 3.

After that, successive approximation procedure (5), (6) was initiated with functions  $z_{\text{depl}}^{(0)}(V)$ ,  $z_{\text{enr}}^{(0)}(V)$  calculated using equation (12). Modification of the numbered dependences  $U_{\text{enr}}^{(n)}(z)$  and  $U_{\text{depl}}^{(n)}(z)$  stopped after 5–6 iterations. From all tunneling electron masses, the best convergence into a single curve was shown by the branch curves  $U_{\text{enr}}^{(6)}(z)$  and  $U_{\text{depl}}^{(6)}(z)$  at  $m = 1.2m_0$ . The curves  $U(z)$  and  $U_{\text{mod}}(z)$  corresponding to this mass are shown in Fig. 4.

The shape of the actual potential pattern in the ultrathin insulating layer similar to that obtained in [7] considerably differs from the rectangular barrier typical of the thick silicon oxides. Its part with a height of  $> 1$  eV is by 40% thinner than  $\text{SiO}_2$  film and the mass of electron that tunnels through it is much greater than  $0.5m_0$ . Assumptions regarding the barrier pattern made before in [8,13] have been also proved. As compared with [7], in this case, the potential pattern in the insulator has a maximum significantly offset to the oxide–polysilicon interface; potential drop towards the semiconductor contact is much more gently sloping that towards poly- $n^+$ -Si.

By comparing the model and actual potential patterns (see Fig. 4), it can be concluded that the model shape cannot be used for a rigorous description of electron wave

<sup>1</sup> This was obtained for some  $m$  values during selection of the barrier height  $U_*$ .

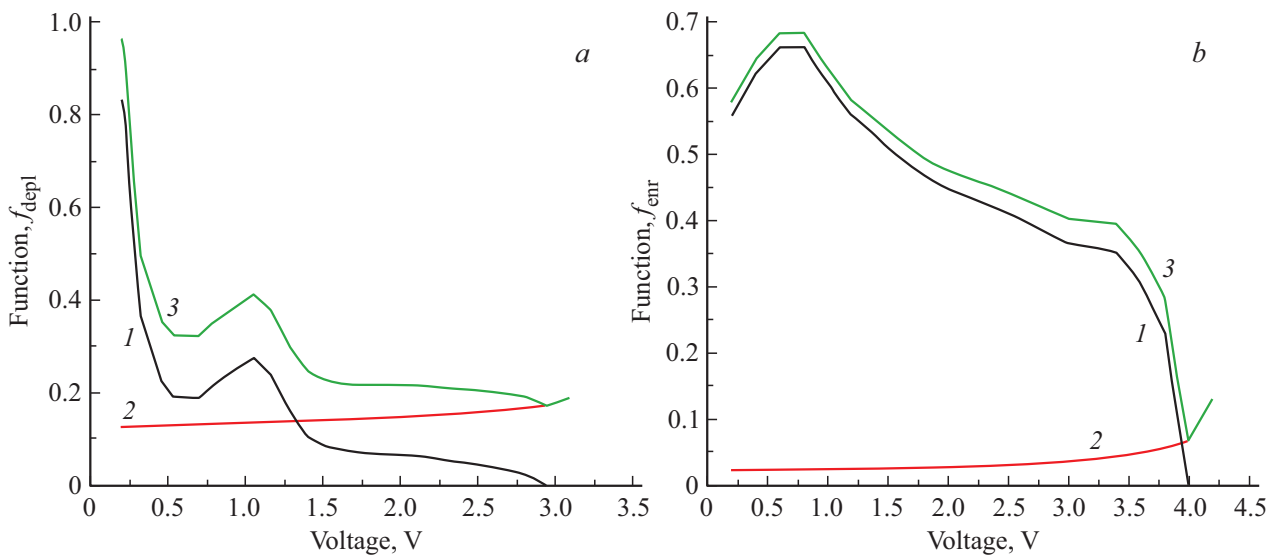


**Figure 3.** Functions  $\tilde{f}(V)$ ,  $\hat{f}(V)$  and  $f(V)$  at  $m = 1.2m_0$ . *a* is the semiconductor depletion branch; 1 —  $\tilde{f}_{\text{depl}}(V)m$ , 2 —  $\hat{f}_{\text{depl}}(V)$ , 3 —  $f_{\text{depl}}(V)$ . *b* is the semiconductor enrichment branch; 1 —  $\tilde{f}_{\text{enr}}(V)m$ , 2 —  $\hat{f}_{\text{enr}}(V)$ , 3 —  $f_{\text{enr}}(V)$ .

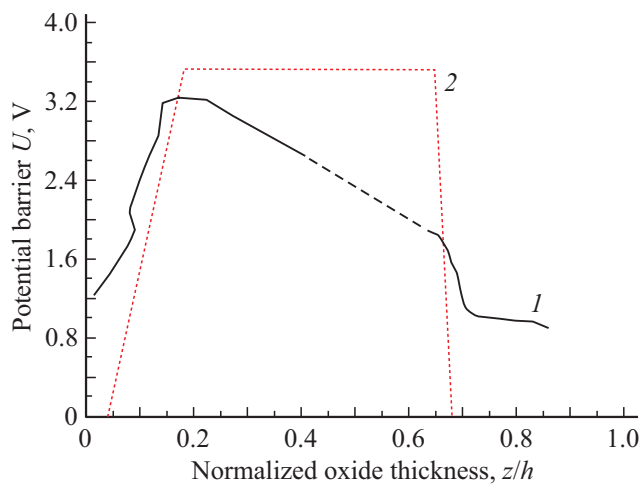


**Figure 4.** The actual and model potential pattern in ultrathin insulating layer. 1 — actual potential, 2 — model potential. Due to the limitations of the maximum branch voltages,  $U_{\text{enr}}^{(6)}(z)$  and  $U_{\text{depl}}^{(6)}(z)$  were not joined. This section on curve 1 is shown as a dashed line.

function penetration into SiO<sub>2</sub> ultrathin insulating layer. This is despite the fact that function (10) with the parameters from the table reflects the features of the potential pattern in ultrathin oxide — barrier offset towards the field electrode contact. The role of the model is only limited to auxiliary functions: to supplement the experimental data — to make dependence  $\hat{f}(V)$  — and to initiate the successive approximation procedure.

**5. Conclusion**

The absence of theoretical grounds for silicon oxide that enable to use the effective mass equation to describe the

electron wave function sets up a task to determine the actual potential pattern in the ultrathin insulating layer by means of experiment. Such task setting makes the task contingent on the method used to prepare a certain sample. However, the actual dependences of the insulating potential vs. coordinates on the normal to the layer plane constructed using the experimental data have several common important properties. The barrier is always significantly thinner than the insulating layer, with its maximum shifted towards the contact with the polycrystalline material, and the effective mass of the tunneling electron is several times greater than the typical for thick silicon oxide  $m = 0.5m_0$ . In order to explain the nature of such potential pattern, layer-by-layer crystallographic investigations of ultrathin SiO<sub>2</sub> structures are required, which are not included in the scope of this research. The obtained data on the insulating potential shape created by the silicon oxide film may be used for calculations of a wide range of nanoelectronic devices.

**Funding**

This study was carried out within the framework of a state assignment and partially supported by the Russian Foundation for Basic Research (RFBR projects No. 18-29-11029-mk, No. 19-07-00271-a and No. 19-29-03042-mk).

**Conflict of interest**

The authors declare that they have no conflict of interest.

**References**

[1] F.A. Zwanenburg, A.S. Dzurak, A. Morello, M.Y. Simmons, L.C.L. Hollenberg, G. Klimeck, S. Rogge, S.N. Coppersmith, M.A. Eriksson. *Rev. Mod. Phys.*, **85** (3), 961 (2013).

- [2] A.P. Baraban, V.V. Bulavinov, P.P. Konorov. *Electronics of layers on silicon* (Leningrad, State University, 1988) p. 303.
- [3] E.H. Nicollian, I.R. Brews. *MOS (Metal Oxide Semiconductor) Physics and Technology* (N. Y., John Willey and Sons, 1982).
- [4] E.E. Tahtomirov, V.A. Volkov. *ZhETH*, **116** (5), 1843 (1999).
- [5] T. Ando, A. Fowler, F. Stern. *Rev. Mod. Phys.*, **54** (2), 437 (1982).
- [6] R. Vasudevan, G. Pilia, P.V. Balachandran. *J. Appl. Phys.*, **129**, 070401 (2021).
- [7] E.I. Goldman, A.G. Zhdan, N.F. Kukharskaya, M.V. Chernyayev. *FTP*, **42** (1), 94 (2008) (in Russian).
- [8] E.I. Goldman, S.A. Levashov, G.V. Chucheva. *FTP*, **53** (4), 481 (2019) (in Russian).
- [9] F. Rana, S. Tiwari, D.A. Buchanan. *Appl. Phys. Lett.*, **69** (8), 1104 (1996).
- [10] A. Hadjadi, G. Salace, C. Petit. *J. Appl. Phys.*, **89** (12), 7994 (2001).
- [11] E.I. Goldman, N.F. Kukharskaya, A.G. Zhdan. *Solid-State Electron.*, **48** (5), 831 (2004).
- [12] E.I. Goldman, A.I. Levashova, S.A. Levashov, G.V. Chucheva. *FTP*, **49** (4), 483 (2015) (in Russian).
- [13] D.A. Belorusev, E.I. Goldman, V.G. Naryshkina, G.V. Chucheva. *FTP*, **55** (1), 24 (2021) (in Russian).